In-situ uniaxial drawing of poly-L-lactic acid (PLLA): Following the crystalline morphology development using time-resolved SAXS/WAXS

Journal Item

In-situ uniaxial drawing of poly-L-lactic acid (PLLA): following the crystalline morphology development using time-resolved SAXS/WAXS

Ellen L. Heeley[a], Kharmen Billimoria[b], Nathan Parsons[b], Łukasz Figiel[b], Elspeth M. Keating[c], Conor T. Cafolla[c], Eleanor M. Crabb[a], Darren J. Hughes[c]

[a]Faculty of Science, Technology, Engineering and Mathematics, Open University, Walton Hall, Milton Keynes, MK7 6AA, UK

[b]International Institute for Nanocomposites Manufacturing (IINM), WMG, University of Warwick, Coventry, CV4 7AL, UK

[c]WMG, University of Warwick, UK, CV4 7AL

Corresponding author: Ellen Heeley (Ellen.Heeley@open.ac.uk)

Abstract

Simultaneous synchrotron small- and wide-angle X-ray scattering (SAXS/WAXS) was used to follow the crystalline morphology evolution of poly-L- lactic acid (PLLA) during uniaxial deformation at various draw temperatures (T_d). The mechanical behaviour of PLLA, was found to be strongly dependent on T_d. 2D SAXS/WAXS data taken during the draw showed that at low T_ds cavitation and voiding occurred and the initial crystallites underwent 'overdrawing' where they slip and are partially destroyed. SEM confirmed that surface voiding and cavitation had occurred at T_d = 60 and 65 ^oC but was absent at higher T_ds. During the draw, no long-range macromolecular lamellar structure was seen in the SAXS, but small crystallites of the disordered α' crystal form of PLLA were observed in the WAXS at all T_ds. The PLLA samples were then step annealed in a second processing stage (post-draw) to develop the oriented crystalline lamellar structure and increase the amount of the stable α crystalline form. SAXS/WAXS data showed that a highly oriented lamellar stack macrostructure developed on annealing, with increased crystallite size and crystallinity at all T_ds. Furthermore, step annealing drove the crystalline transition in all samples from the disordered α' crystal form to the stable α crystal form. Therefore, varying pre- and post-processing parameters can significantly influence the mechanical properties, orientation, crystalline morphology and crystal phase transition of the final PLLA material.

Key words

Poly-L-lactic acid; uniaxial deformation; SAXS/WAXS; crystalline morphology; orientation.

1. Introduction

Poly-lactic acid (PLA) is a compostable thermoplastic biopolymer derived from renewable resources such as corn starch and sugar cane [1, 2]. It has many uses and applications in biomedical devices and tissue engineering due to its biocompatibility and bioresorbability, being safely metabolised by the body [3, 4]. As PLA is a biodegradable thermoplastic polymer with good mechanical and processability, optical and thermal properties it is attracting great interest in textile and packaging industries as a replacement for petrochemical plastics [5-7]. However, like any petroleum-based polymer, the mechanical and physical properties of PLA are dictated by its crystalline micro- and macrostructure. These properties are introduced into a polymer via well-established polymer-manufacturing techniques; e.g. melt processing via extrusion, injection moulding, casting, fibre spinning film blowing and thermoforming [7, 8]. Thus, understanding and controlling the crystallization and structure development in PLA, is fundamental in expanding its commercial applications.

PLA has two enantiomeric forms, poly-D-lactic acid (PDLA) and poly-L-lactic acid (PLLA) [9]. PLLA has a semi-crystalline structure and therefore is the more mechanically stable, whilst PDLA is usually amorphous. To control the crystallinity in PLLA low amounts (≤2%) of the D-form improves the processability of the PLLA but reduces the melting point and the crystallinity, and at levels of ~12% D-form content the polymer can become completely amorphous [1, 4]. Therefore, the crystalline structural evolution in PLLA is a function of the D-form content as well as the processing method employed, e.g. increasing the orientation of the molecular chains by applying strain and thermal treatment can increase the crystallinity. However, this can be a challenging task due to the various of crystalline forms that exist and the slow crystallization rate of PLLA [8].

Depending on the processing conditions PLLA can crystallize in three main forms, α, β and γ [8, 10]. The α crystal form is the most common and stable, developing from melt and solution cooling. The α form has an orthorhombic unit cell (a = 10.7 Å, b = 6.45 Å, c = 27.8 Å), with a 10_3 helical chain conformation [11]. The β crystal form is a less common and is obtained when the α form of PLLA is deformed to high draw ratios such as during fibre spinning processing [12, 13]; this form has an orthorhombic unit cell (a = 10.3 Å, b = 18.2 Å, c = 9.0 Å) and a 3_1 helical chain formation [13]. Further to the α and β forms, a disordered α' form is common in PLLA, having the same crystal lattice of the α form but is more disordered with reduced chain packing [10]. This form is observed when PLLA is crystallized below 120 °C, and is a precursor to the ordered α form [14, 15]. The γ form of PLLA is considered an

obscure phase, with an orthorhombic unit cell (similar to the oriented β phase), and is obtained from epitaxial crystallization on hexamethylbenzene [16, 17].

Increasing the α crystal form in PLLA during processing is desirable to improve the crystallinity and mechanical properties of the polymer. Many studies have focused on the strain-induced crystallization of uniaxial and biaxial deformation of amorphous PLLA at different draw temperatures (T_d) and strain rates [18-23]. However, fewer studies have investigated the crystalline structure development and orientation of PLLA having been pre-crystallized before processing. Of these, Zhang *et al* [24] pre-crystallized PLLA to induce the α crystal form before uniaxial deformation and concluded that stress and T_d are significant factors in cavitation formation in the samples. Wang *et al* [25] investigated the crystalline structure by varying T_d and strain rate on pre-crystallized PLLA samples. Wide-angle X-ray scattering (WAXS) analysis showed that highly oriented crystallites formed at low initial crystallinity due to strain-induced crystallization effects and greater orientation is seen at lower T_d due to slower chain relaxation in the PLLA. Renouf-Glauser *et al* [26] looked at the uniaxial deformation of both amorphous and annealed PLLA using small-angle X-scattering (SAXS). The pre-crystallized PLLA, showed the development of a 'lemon-peanut' shaped SAXS pattern, relating to a cavitation and fibrillated structure. Failure of samples during deformation was due to crazing and cavitation and the crystalline structure only controlled the extent of deformation.

Previously, we have reported on the effect of strain rate and draw temperature on the crystalline structure of uniaxially drawn amorphous PLLA using SAXS/WAXS, thermal and SEM analysis techniques [27]. We applied secondary processing via step annealing to the post-drawn PLLA samples in order to develop the crystalline morphology and enhance the α'- α crystalline form transition. Our initial work indicated that T_d has a significant effect on the formation of the α form where T_ds between 60-80 ^oC induced the α' form, but at $T_d \geq 90$ ^oC, the α form was obtained directly post-draw. Hence, the temperature range considered in this work (T_ds between 60-75 ^oC) is around the glass transition temperature. This temperature window is typical in secondary processing (or quasi solid-state processing) of thermoplastic polymers such as injection-stretch blow moulding or film blowing. Here, we present further insight into the mechanical behaviour and crystalline morphology evolution of pre-crystalline PLLA during uniaxial deformation using simultaneous synchrotron small- and wide-angle X-ray scattering (SAXS/WAXS) throughout the draw at a 400 ms acquisition time. Additionally, we then subjected the samples to secondary processing via step annealing,

whereby the evolution of the oriented long-range lamellar morphology and α'- α crystalline form transition was also followed. Hence, determining the pre- and post-processing parameters that significantly influence the mechanical properties, orientation, crystalline morphology and crystal phase transition of the final PLLA material.

2. Experimental

2. 1 Materials and Sample Preparation

Commercial Poly-L-lactic acid (PLLA) Luminy L175, was purchased from Total Corbion (Netherlands) with the L-isomeric content being ≥ 99 %. The average M_w = 136 kDa, M_n = 43 kDa and polydispersity = 3.2 was determined from GPC measurements [27]. Before use the PLLA pellets were dried for 12 hours at 60 °C and then extruded using a HAAKE^{TM} Minilab 2 twin-screw compounder (Thermo Fisher Scientific, Massachusetts), at 120 rpm and a temperature of 180 °C. PLLA was then hot injection moulded using a HAAKE^{TM} Minijet at 180 ^{o}C and 600 bar with a mould temperature of 65 ^{o}C, to produce rectangular samples for tensile testing. Once cooled, samples were stored under ambient conditions. DSC measurements on the processed PLLA determined the values of T_g and T_m at 61 ^{o}C and 175 °C respectively, with a sharp cold crystallisation T_{cc}, peak between 94 – 107 ^{o}C [27].

2.2 Mechanical Testing

In-situ tensile testing was performed using a computer controlled Instron 3367 tensile testing instrument, fitted with a custom-made thermostatic chamber and a 30 kN load cell (as shown in Figure 1A). Non-standard rectangular tensile samples with the following dimensions were used: gauge length 10 mm, width 5 mm, and thickness 1 mm. The tensile tests were carried out at the constant nominal strain rate of 10 mm min^{-1}, and an isothermal draw temperature (T_d) range from 60 °C to 75 °C. Samples were extended to 100% of their original gauge length, or until failure. Engineering stress (σ_n) and strain (ε_n) values were converted to true stress (σ_T) and true strain (ε_T) as follows; $\sigma_T = \sigma_n(1 + \varepsilon_n)$ and $\varepsilon_T = \ln(L/L_0)$, where L is the gauge length at a given time during the test, and L_0 is the original gauge length.

2.3 Thermal analysis

Differential Scanning calorimetry (DSC) was performed on the undrawn and drawn-annealed PLLA samples using a DSC1 STARe instrument (Mettler Toledo, USA). Samples of 2-7 mg were sealed into standard 40 µL aluminium pans. The heat-cool cycles were carried out under

a nitrogen atmosphere (50 mL min^{-1}) from 25 – 200 °C at a heating rate of 10 °C min^{-1} and from 200 – 25 °C at cooling rate of 10 °C min^{-1}.

2.4 In-situ SAXS/WAXS measurements using synchrotron radiation

Simultaneous two-dimensional SAXS/WAXS measurements were performed on beamline I22 of the Diamond Light Source, UK [28], with an X-ray energy of 12.4 keV. Uniaxial drawing of the PLLA samples was performed using the Instron tensile testing instrument as described above (as shown Figure 1A and 1B), which was custom-designed to fit the beamline [29]. This instrument was positioned on the beamline and samples were secured in place via a grip system and located central to the X-ray beam position (Figure 1B and 1C). A vacuum chamber (reducing air scattering and absorption) was positioned between the thermostatic sample chamber and a Pilatus P3-2M SAXS detector with a sample to detector distance of 5.8 m. A Pilatus P3-2M-DLS-L WAXS detector was located at a sample-to-detector distance of 225 mm. The SAXS and WAXS detectors were calibrated with a 100 nm diffraction grating and silicon powder, respectively.

The PLLA samples were heated to a draw temperature T_d between 60 – 75 °C and soaked for three minutes before drawing at each T_d. Samples were then drawn at a strain rate of 10 mm min^{-1} to 100% elongation and simultaneous SAXS/WAXS data was acquired at a frame rate of 1 s (400 ms collection and 600 ms dead time) throughout the 60 s draw. Once the draw was complete, samples were then step annealed at temperatures between 90 – 160 °C: samples were heated to the annealing temperature and then held at that temperature for 180 s. Once annealed, SAXS/WAXS data was taken at a frame rate of 400 ms at each annealing temperature.

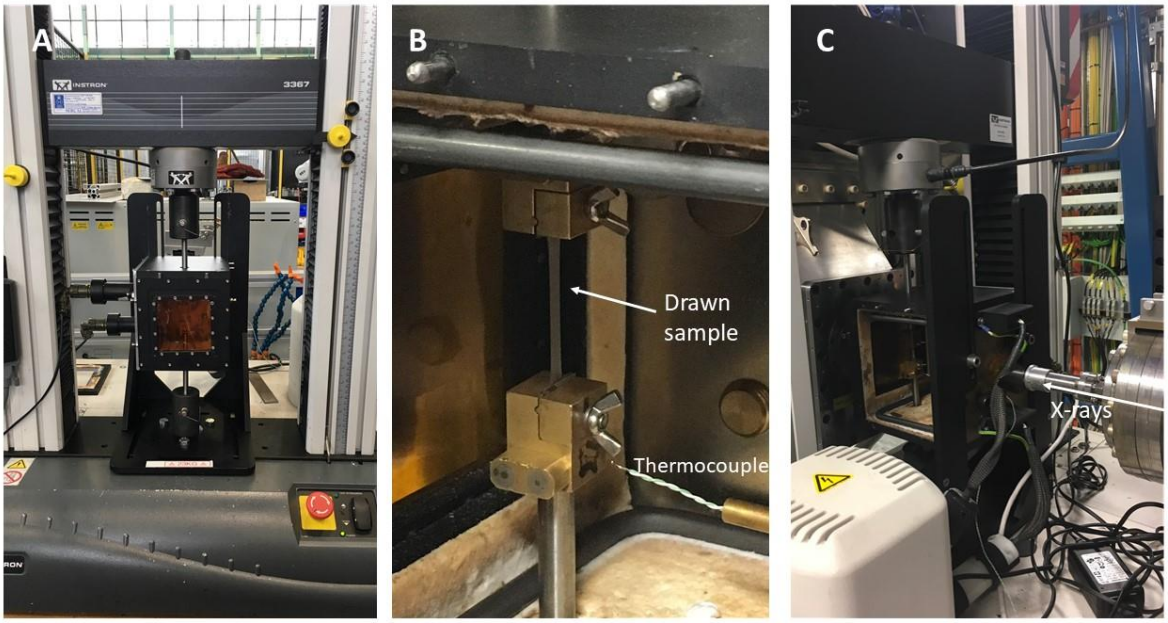

Figure 1. *In-situ* tensile testing instrumentation. **A**: Instron instrument with thermostatic hearting chamber; **B**: Inside of the thermostatic heating chamber showing a drawn PLLA sample; **C**: Instron instrument with thermostatic heating chamber positioned on I22 beamline (Diamond, Light Source UK).

2.4.1 SAXS/WAXS data analysis.

2D SAXS/WAXS data reduction and analysis was performed using DAWN [30, 31] and CCP13 Fibrefix [32], software suites. Data were normalized for sample thickness, transmission and background scattering.

The 2D SAXS/WAXS data were reduced to 1D profiles of intensity (I) versus scattering vector (q) (where $q = (4\pi/\lambda)\sin(\theta)$, 2θ is the scattering angle and λ is the X-ray wavelength), from meridional sector integrations averaged symmetrically around the draw direction, at a fixed angle and radius, q. Radial azimuthal 1D profiles were obtained from the 2D SAXS data at fixed radius q from the angular variation in intensity, over an azimuthal angle φ, range of 0 - 360°(i.e. $I(q, \varphi)$). The resulting two peaks in the 1D SAXS azimuthal profiles were then fitted using Lorentzian functions to obtain the average full width half maximum (FWHM) allowing the relative orientation changes of the lamellar stacks to be determined.

Correlation functions were computed from the 1D meridional SAXS scattering profiles using the Corfunc software routines [33] incorporated into the SasView SAXS analysis package [34]. The 1D correlation function, $\gamma(R)$, is expressed as:

$$\gamma(R) = \frac{1}{Q_s}\int_0^\infty I(q)q^2\cos(qR)\mathrm{d}q \quad (1)$$

where $I(q)$ is the scattering intensity and Q_s is the experimental invariant obtained from the 1D SAXS profile between the experimental limits of q_1 (first data point) and q_2 (region where $I(q)$ is constant). The experimental invariant is expressed as:

$$Q_s(t) = \int_0^\infty q^2 I(q)\mathrm{d}q \approx \int_{q_1}^{q_2} q^2 I(q)\mathrm{d}q \quad (2)$$

Correlation functions were computed via the extrapolation of the 1D SAXS data ($q \rightarrow \infty$) according to Porod's law [35] and a Guinier model back extrapolation ($q \rightarrow 0$) [36]. The correlation function analysis assumes an ideal two-phase lamellar morphology [36, 37] where various parameters including long period, L_p, crystalline layer thickness H_b, and estimated local percent crystallinity X_c can be extracted [33].

2.5 Scanning electron microscopy measurements

Scanning Electron Microscopy (SEM), was performed using a TM3030 Plus table-top instrument (Hitachi High-Technologies, Tokyo, Japan). All samples were imaged without surface preparation using back-scatter electron (BSE) detection at 5 kV.

3. Results and discussion

3.1 Mechanical testing

Figure 2 shows representative true stress-true strain data at different draw temperatures (T_d), just below and above the glass transition of the PLLA (T_g = 61 ^{o}C) [27]. Generally, one can distinguish some characteristic regimes for PLLA within the temperature range of interest. In particular, the polymer shows a typical glassy response at T_d = 60 °C with a significant stress drop (around 10 MPa) and associated strain softening behaviour. The origin of yield drop in a glassy polymer near the glass transition is understood as plastic strain-induced structural evolution, called *rejuvenation* [38]. The yield drop is followed by the onset of strain hardening at the value of true strain beyond 0.2. It is noteworthy to mention that the PLLA fails at the true strain of around 0.45 (i.e. before reaching the maximum nominal strain of 1) at T_d = 60 ^{o}C.

At T_d 65 -70 °C, there is an absence of yield peak in this temperature regime, but the material is still retaining some unrelaxed glassy contributions, as indicated by the significant gradient

of the initial portion (up to around ~0.02 of true strain) of the stress-strain curve. Additionally, the onset of strain hardening behaviour starts at around 0.05 of the true strain, and it is characterised by a relatively steady increase in true stress with increasing strain.

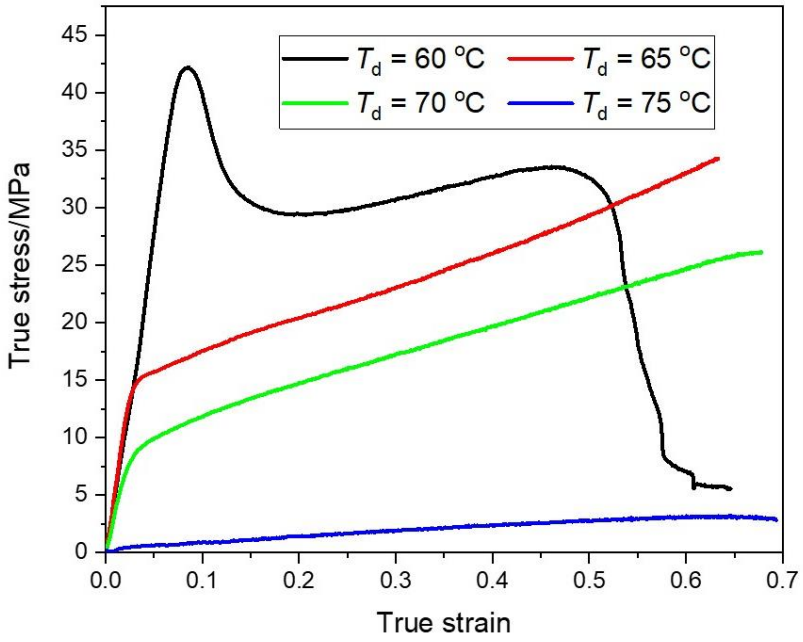

Figure 2. True stress – strain curves for PLLA drawn at T_d between 60 – 75 °C.

At T_d = 75 °C the PLLA seems to exhibit the behaviour of an elasto-viscous melt with some strain hardening. This is the regime where the PLLA response can be described as being governed by the stresses arising from the perturbation of conformational entropy of the entangled chain network, with possible modifications of the deformation behaviour arising from the stress-induced pre-crystallisation [38].

From the mechanical testing data, it can be seen that idealised stress-strain behaviour is observed in the region of T_d 65-70 °C, whereas at T_d = 60 °C (just below T_g), significant yielding is observed; similar results have been observed in PLLA during drawing and temperature between 60 – 80 °C [39]. The mechanical response at different T_ds, can be understood by following the micro- and macrostructure development during drawing, which can be observed from time-resolved SAXS/WAXS during *in-situ* uniaxial drawing of the polymer, which is covered in Section 3.3.

3.2 Thermal analysis

Thermal analysis gives initial information of the melting and crystallization temperatures and bulk crystallinity with respect to T_d. Figure 3 shows the DSC thermograms of the heat-cool

cycles of the drawn and annealed PLLA. In the heating cycle, Figure 3A, the glass transition temperature T_g can be seen at around 61 ^oC for all samples. Table 1 gives the melting temperature T_m, crystallization temperature T_c and percent bulk crystallinity X_c, for all PLLA samples obtained from the DSC thermograms in Figure 3.

Table 1. Thermal data: T_m, T_c and X_c obtained from DSC thermograms for PLLA drawn at T_d between 60 – 75 ^oC.

T_d/ ^{o}C	T_m/^{o}C	T_c/ ^{o}C	X_c/%
60	176	98	30
65	176	97	30
70	177	97	32
75	177	95	40

The melting temperature T_m is 176 – 177 ^oC for all the drawn-annealed PLLA samples and no significant change is seen with respect to T_d. There is a small crystallization peak observed before the melting peak, at 162 ^oC, for T_d = 60 and 75 ^oC, which has been attributed to the transition of the disordered α′ to the more ordered α crystal form before melting [40-43]. Furthermore, the DSC heating thermographs do not show any cold crystallization peaks (T_{cc}), which is common in pre-processed PLLA [27, 41, 44]. The heat-cool DSC thermograms for the as-processed undrawn PLLA is given in Figure S1 of the supplementary material; as with the drawn PLLA, there is no obvious cold crystallization peak and the value of T_m = 176 ^oC. Hence, drawing of the PLLA has no effect on T_m compared with the undrawn PLLA. Similarly, there is no T_{cc} observed so the sample has some crystallinity induced by the processing technique used (this is confirmed later in the SAXS/WAXS analysis).

The percentage bulk crystallinity (χ_c) was calculated for the drawn PLLA samples from the DSC heating curves using the following equation:

$$x_c = \frac{\Delta H_m}{\Delta H_m^0} \times 100 \qquad (3)$$

where ΔH_m, is the enthalpy change during melt, and ΔH_m^0 is the theoretical enthalpy change that occurs from the melting of 100 % crystalline PLLA, having a value of 93 J g^{-1} [45]. From the results listed in Table 1, the crystallinity is seen to increase with increasing (T_d >65 ^oC), as previously observed in this annealing temperature range [27]

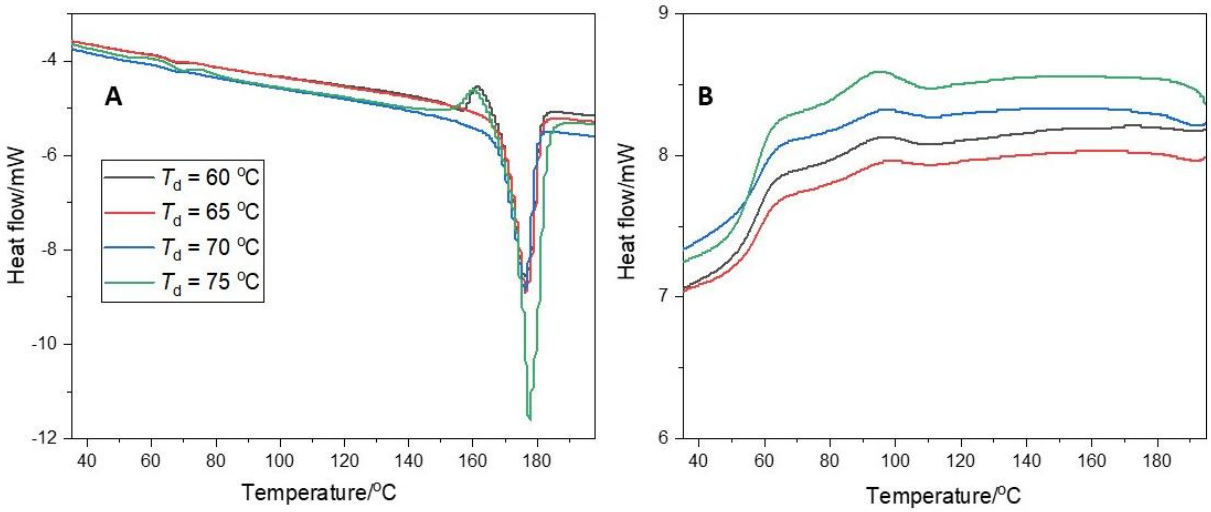

Figure 3. DSC thermograms of PLLA samples drawn at T_d between 60 – 75 °C and annealed at 160 °C; **A**: heating cycle and **B**: cooling cycle.

Figure 3B shows the cooling cycle for all samples. A very broad crystallization peak T_c, is observed at ~97 °C (also seen in the as-processed undrawn PLLA in Figure S1), showing that some crystallinity does return in the samples at a cooling rate of 10 °C min^{-1}. This is not usually observed for PLLA at this cooling rate, due to the slow crystallization kinetics of the material [46, 47]. This would suggest that the processing conditions and annealing treatment produces some residual nucleation sites which prevail from the melt to induce some crystallization on cooling [48].

3.3 Time-resolved SAXS/WAXS data during drawing of PLLA

To relate the morphology and crystalline structure development, 2D simultaneous SAXS/WAXS data was taken before and throughout the drawing process. Firstly, the samples were soaked for three minutes at each draw temperature before drawing. SAXS/WAXS data was taken prior to the draw to evaluate the initial morphology of the samples. Figure 4A, shows the 2D SAXS/WAXS patterns of the samples at T_d between 60 – 75 °C. Generally, there is little macrostructure observed in the 2D SAXS, which is confirmed in Figure 4B, where the 1D profiles show no peaks, other than at 70 °C where a very broad peak appears to have developed at q ~ 0.02 – 0.04 Å^{-1}. Comparing the 2D WAXS at all temperatures, there are oriented diffraction spots on the equator of the patterns. The 1D profiles in Figure 4C, show that the PLLA has an initial crystalline structure where the peaks can be indexed to be a mixture of the α′/α crystal forms.

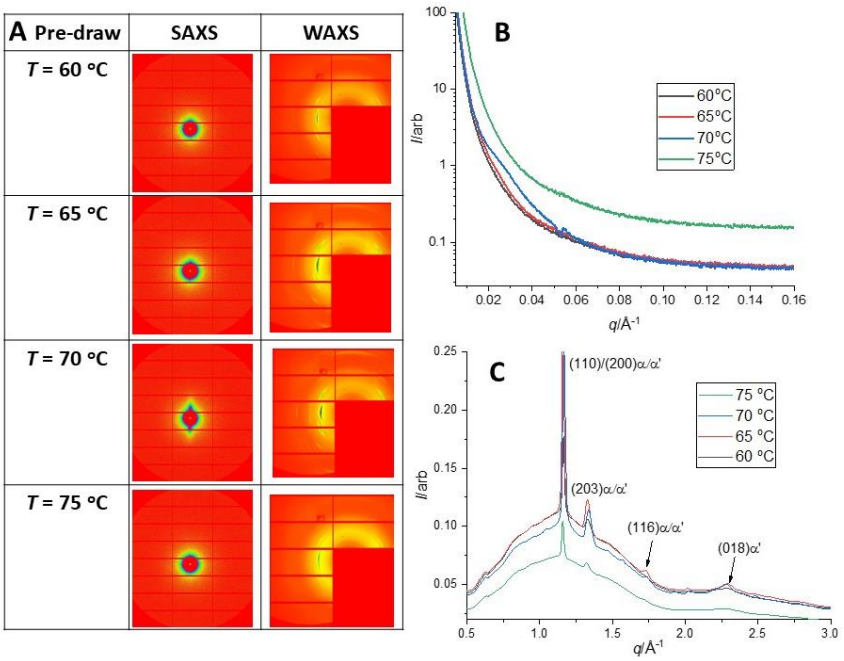

Figure 4. A: 2D SAXS/WAXS patterns pre-draw at T_d between 60-75 ^oC; **B**: corresponding 1D SAXS profiles and **C**: corresponding 1D WAXS profiles.

The initial crystalline structure of the PLLA is also confirmed in the DSC as no cold crystalline peak is observed in the undrawn sample (Figure S1). Hence, the initial injection moulding processing of the PLLA material followed by soaking of the sample at each T_d, can induce some crystallinity in the samples before drawing (observed from the presence of the peaks in the 1D WAXS profiles relating to the α′/α crystal forms). However, no long-range lamellar structure is established, from the lack of ordered SAXS. Further to this, Figures S2 and S3, show the 1D SAXS/WAXS profiles of the as-processed undrawn PLLA; the SAXS again shows no long-range structure is present in the PLLA, but the WAXS does show the main (110)/(200) and (203) peaks for the α′ crystal form. Thus, there are some initial crystallites formed in the sample when processed and are identified as the disordered α′ crystal form.

To determine the structure development during the drawing process, 2D SAXS/WAXS patterns were taken every second throughout the draw. Figure 5A, shows selected frames of 2D SAXS patterns at T_d between 60 – 75 ^oC, (where the draw direction is vertical in all cases). At T_d = 60 ^oC, there is a small change in the intensity in the draw direction after yield around 8 s (see Figure 5B which gives 2D SAXS at points on the tensile curve), this develops as the draw continues. Similar behaviour has been observed in PLLA and other semi-crystalline polymers where initial voiding occurs in the amorphous regions after yield perpendicular to the draw direction [24, 49, 50]. As the draw continues (beyond 30 s),

increased scattering appears perpendicular to the draw direction (on the equator) around the central beam stop and is attributed to increased formation of cavities and voids forming parallel to the draw direction [23, 24]. At T_d = 65 ^oC scattering develops in the draw direction (small lobes form), indicating that some long-range crystalline structure develops perpendicular to the draw direction. As the draw continues the scattering from the lobes tends to decrease and slightly increased scattering is seen in the equatorial direction indicating some voiding occurs. However, at T_d = 70 ^oC, lobes in the draw direction develop early on, again indicating some long-range crystalline structure is present (as seen in the undrawn samples in Figure 4A), but these lobes tend to move into the beam stop position from 30 s into the draw (see Figure 5C which shows 2D SAXS patterns at points on the tensile curve at T_d = 70 ^oC). Here, the amorphous chains orient and the initial crystallites slip and are partially destroyed, as the draw enters the strain hardening region [23, 24]. Conversely, at T_d = 75 ^oC, the SAXS patterns show no structure throughout the draw. At this higher draw temperature the amorphous chains have greater mobility and are elongated to a greater extent throughout the draw and no cavitation occurs [42].

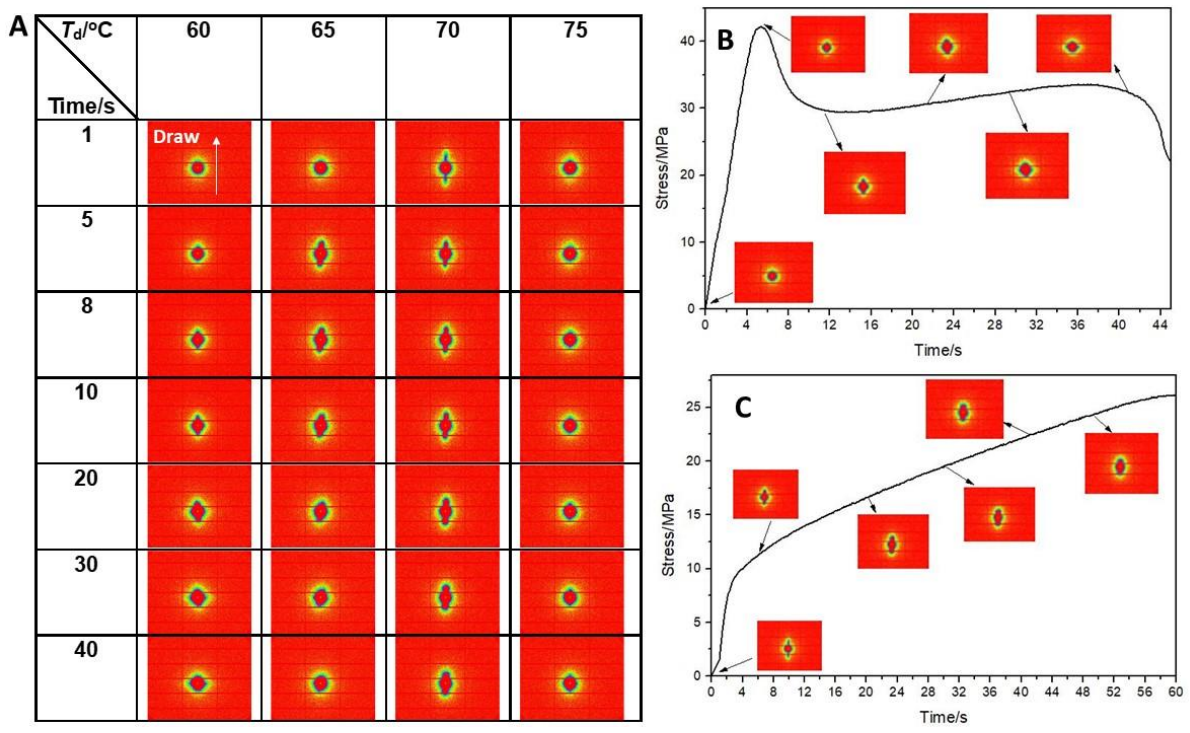

Figure 5. A: Selected 2D SAXS patterns during the 60 second draw period at T_d between 60 – 75 ^oC; 2D SAXS patterns corresponding to various points on the mechanical testing curve for; **B**: at T_d = 60 ^oC and **C**: at T_d = 70 ^oC. (The draw direction is vertical in each pattern.)

To gain a greater insight into the crystallite slip process, 2D WAXS was also obtained throughout the drawing process. Figure 6, shows selected frames of 2D WAXS patterns at T_d

between 60 – 75 °C, (the draw direction is vertical in all patterns). Initially, at 1s into the draw, with T_d between 60 – 75 °C, all samples show an oriented crystal structure with intense scattering arcs of the (110)/(200) planes indicating a mixture of the α′/α crystal forms (as indicated in Figure 4C). At T_d 60 – 70 °C, as the draw progresses, the (110)/(200) scattering arcs become broader indicating that the crystallites have lost some orientation. Hence, as the crystallites are drawn, they slip, and partial destruction occurs leading to a breakdown in orientation being observed at lower T_ds. This trend has been reported during uniaxial drawing of PLLA, being referred to as 'over-drawing' [23, 25, 44]. Figure S4, shows 2D WAXS patterns at various points on the stress-strain curve for T_d = 60 °C. Before and after yielding the WAXS patterns show arcs of intensity on the equator (perpendicular to the draw), indicating oriented crystallites in the PLLA. Beyond the yield peak in the strain hardening region, the equatorial arc intensity becomes more diffuse (increase in azimuthal spread), indicating the overdrawing of the sample and reduction in orientation of the crystallites.

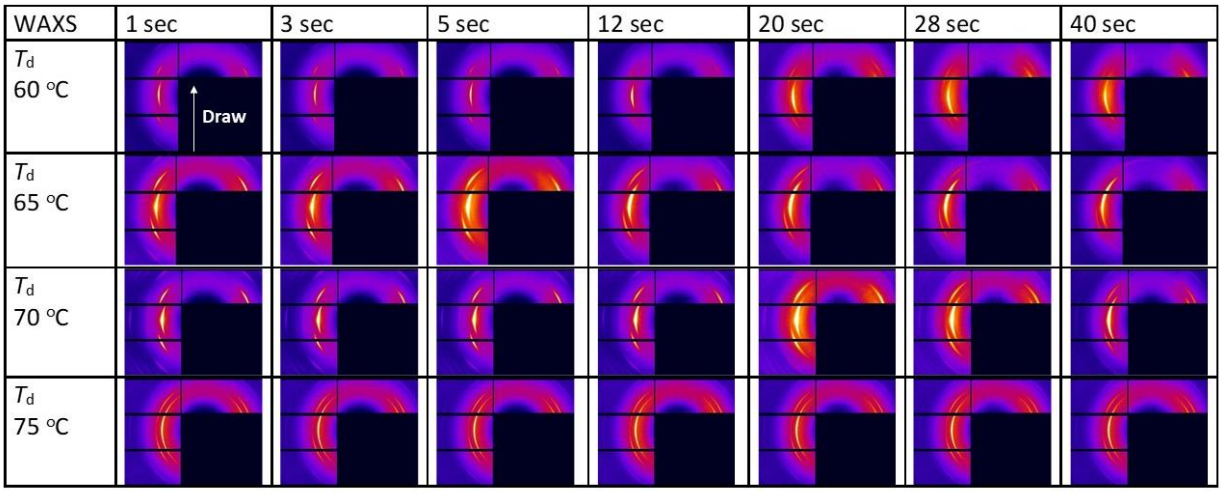

Figure 6. Selected 2D WAXS patterns during the 60 second draw period at T_d between 60 – 75 °C. (The draw direction is vertical in each pattern.)

3.4 SEM of PLLA samples

The surface of the PLLA samples post-draw were examined to determine if any surface crazing has occurred and to confirm the evolution of voiding and cavitation. Figure 7 shows the SEM images of PLLA samples drawn at T_d between 60 -75 °C for 60 s, where the draw direction is horizontal (as indicated in the figure) in all cases. At T_d = 60 °C, large crazing and

cavitation in the sample is observed perpendicular to the draw direction. As this temperature, is below T_g, the molecular motion of the molecules is restricted and so cavities occur more easily in the amorphous regions and stress whitening occurs [50]. This is also confirmed in the 2D SAXS (Figure 5A and 5B), where, as the draw proceeds after yielding, some equatorial scattering is seen to develop from this cavitation. For the sample drawn at T_d = 65 ^oC, some voiding and cavitation is also observed in the SEM surface image (Figure 7B). At T_d between 70-75 ^oC (Figure 7C and 7D), the surface appears much smoother with a lack of voiding, again this fits with the 2D SAXS, where the equatorial scattering is reduced or does not occur to any extent.

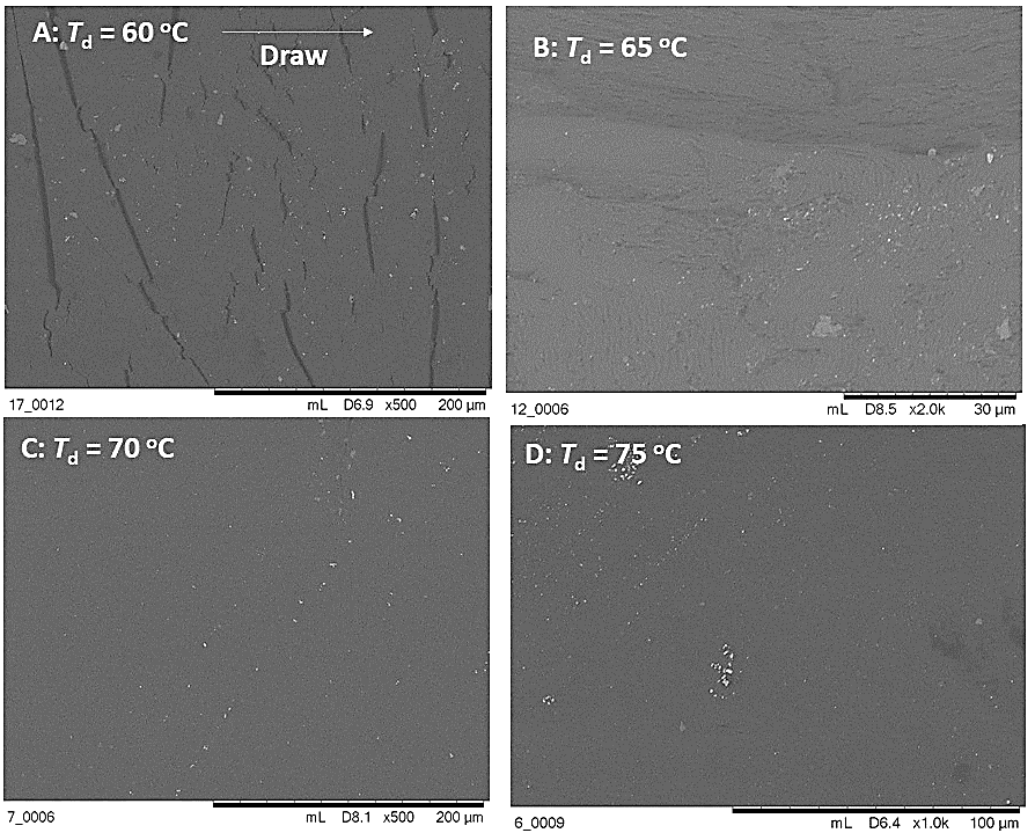

Figure 7. SEM surface images of PLLA post-draw after 60 s, where the draw direction is horizontal in all images. **A**: T_d = 60 ^oC; **B**: T_d = 65 ^oC; **C**: T_d = 70 ^oC and **D**: T_d = 75 ^oC.

3.5 Structure development during annealing post-draw from SAXS/WAXS

The crystalline structure and orientation post-draw can be developed by step annealing the PLLA samples. Figure 8 shows the 2D SAXS/WAXS patterns at each draw temperature step annealed from 90 to 160 ^oC. The 2D SAXS patterns reveal that at all draw temperatures, a distinct spot-like intensity develops in the draw direction, which is indicative of a well-oriented lamellar morphology [14, 27, 51]. As the annealing temperature increases, the spots

collapse into the central beam stop, which indicates an increase in the average lamellar-amorphous repeat distance. The 2D WAXS patterns post-draw at T_d between 60 -75 ^oC, and annealed at 90 ^oC, show the diffraction arcs of the α′/α crystal forms of PLLA, indicating that the crystallites are oriented in the draw direction (as part of the larger lamellar crystalline layers). As the annealing temperature increases the diffraction arcs start to reduce in azimuthal angle and become more centred on the equator, indicating that the orientation and crystallite perfection is developing within the sample. However, at T_d = 75 ^oC, the crystallites appear to be less well oriented at 90 ^oC as these diffraction arcs have greater spread in azimuthal angle, and even during annealing there seems little change in the orientation and crystal perfection of the crystallites. However, the relative orientation of the lamellar stacks during annealing can be determined by further analysis of the 2D SAXS patterns.

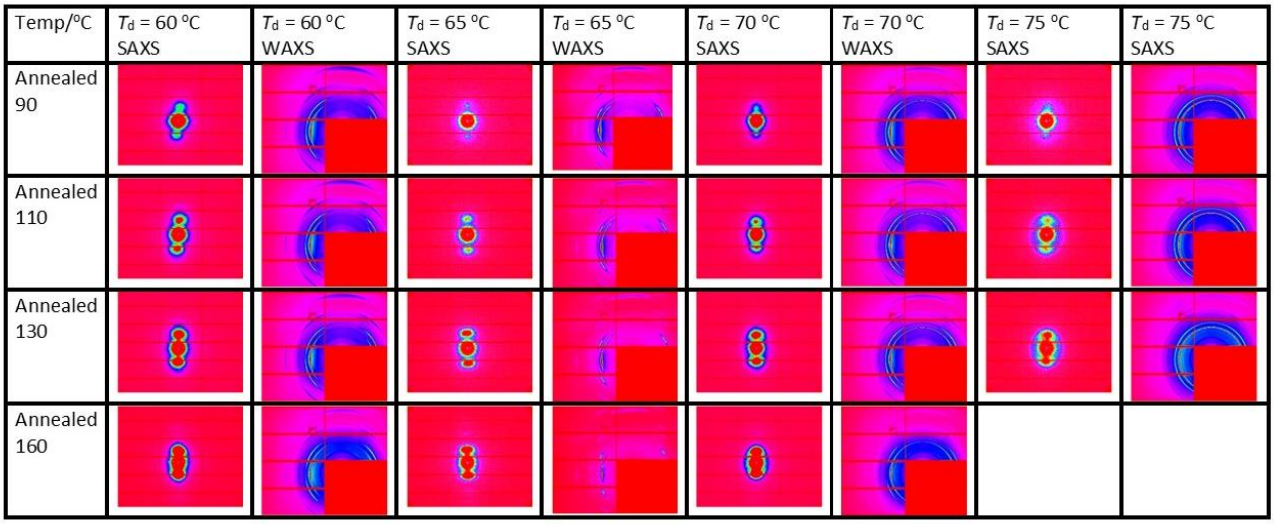

Figure 8. 2D SAXS/WAXS patterns of post-drawn PLLA at T_d between 60-75 ^oC, then step annealed from 90 ^oC to 160 ^oC. (The draw direction is vertical in all images.)

3.5.1 Development of lamellar stack orientation post-draw during annealing

To obtain a more quantitative understanding into how the lamellar stack orientation develops in the PLLA samples during the step annealing process, 1D azimuthal profiles of the 2D SAXS were taken and fitted using a Lorentzian function to obtain the FWHM of the peaks.

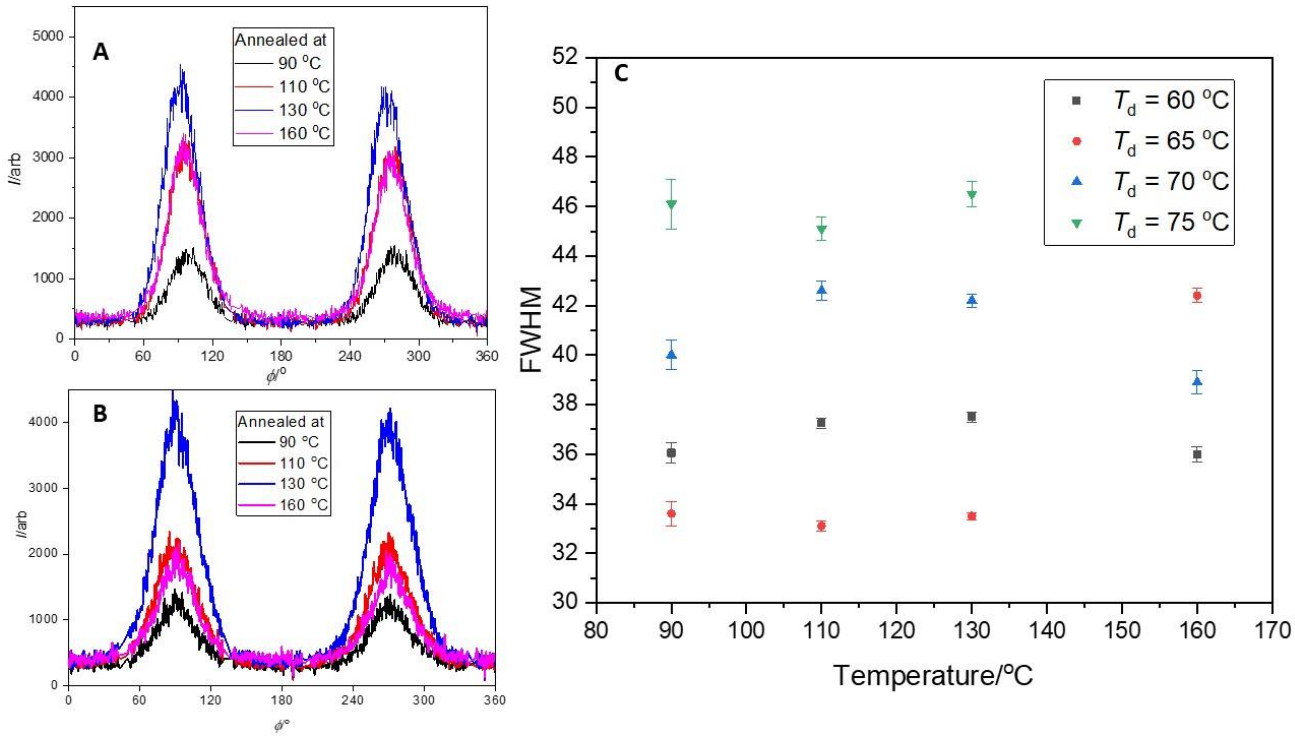

Figure 9. Development of 1D SAXS azimuthal profiles of PLLA during step annealing; **A**: drawn at T_d = 60 °C; **B**: T_d = 70 °C. **C**: change in FWHM for drawn PLLA at T_d between 60 – 75 °C during step annealing.

Figure 9A and 9B, show example 1D SAXS azimuthal profiles of PLLA drawn at T_d = 60 °C and T_d = 70 °C and then step annealed, respectively (similarly Figure S5, shows the 1D SAXS azimuthal profiles of PLLA drawn at T_d = 65 and 75°C). The azimuthal profiles show two distinct peaks which develop during the annealing process. The development of the lamellar stack orientation during the annealing process for all samples was obtained from the average FWHM of the peaks and is shown in Figure 9C (note Figure S6, shows an example of the Lorentzian peak fitting of the 1D SAXS azimuthal profile to obtain the FWHM for PLLA draw at T_d = 60 °C and annealed at 130 °C). In Figure 9C, a reduction in FWHM indicates an increase in orientation. Generally, the lamellar stack orientation for all samples does not change significantly with increasing annealing temperature. However, the draw temperature has a significant effect on the overall orientation, with the greatest seen at T_d = 60 and 65 °C, then decreasing with T_d = 70 °C. The least lamellar stack orientation is seen at T_d = 75 °C, which is confirmed in the 2D WAXS (Figure 8), where the spread in azimuthal angle of the diffraction arc is evident at this draw temperature. The reduction in orientation is expected at the higher T_d's (70-75 °C), as at these temperatures the molecular chains are more mobile (being up to 15 °C above T_g) and can relax [27, 52] and so the lamellar stacks grow with a greater variation in orientations around the draw direction.

3.5.2. Crystalline morphology development: correlation function analysis of 1D SAXS

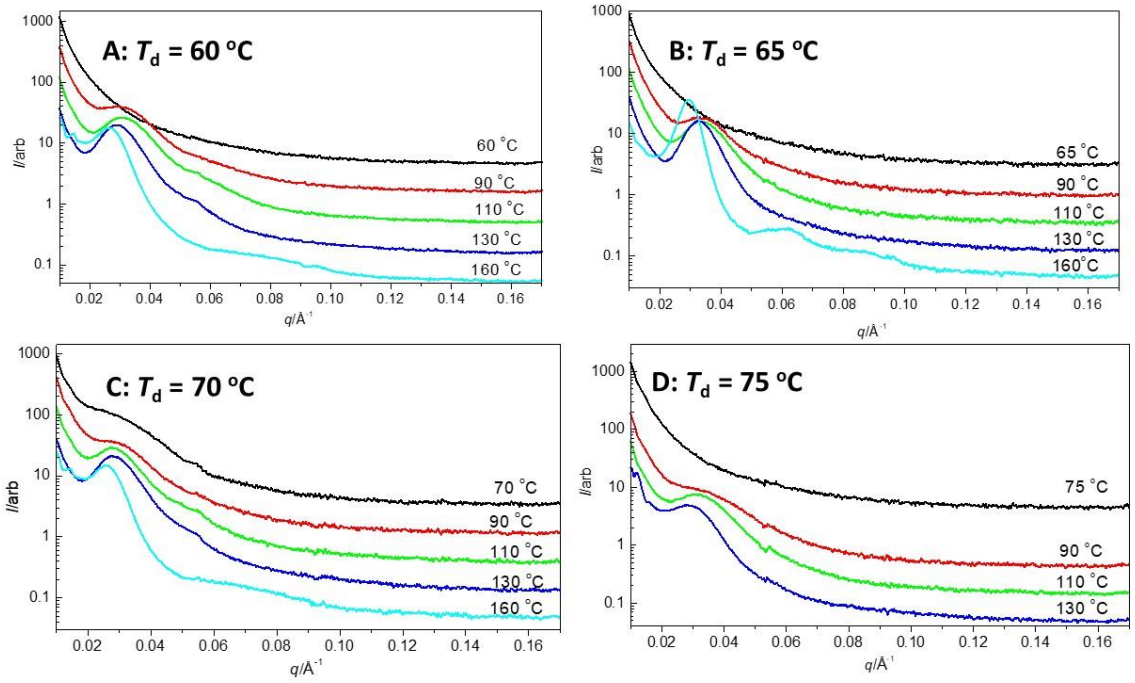

Figure 10. 1D SAXS meridional profiles of PLLA during step annealing; **A**: T_d = 60 °C; **B:** T_d = 65 °C; **C**: T_d = 70 °C and **D**: T_d = 75 °C.

To investigate the crystalline morphology development during step annealing of the drawn PLLA samples, a detailed analysis of the 1D meridional SAXS data was carried out. Figure 10A – 10D, shows the development of the 1D SAXS meridional profiles of the drawn PLLA at T_d between 60 – 75 °C, and during step annealing from 90 – 160 °C. At each T_d, the 1D SAXS profiles show no apparent structure development post-draw, except at T_d = 70 °C, where a very broad peak is observed at q = 0.02 – 0.05 Å^{-1}, indicating the emergence of the long-range lamellar crystalline morphology in the draw direction. At an annealing temperature of 90 °C, all samples show the development of a broad SAXS peak with a peak between q = 0.03 – 0.04 Å^{-1}. As the annealing temperature increases this peak is seen to shift to lower q values in all samples with a reduction in the width of the peak. At annealing temperatures between 110 – 160 °C and T_d between 60 – 70 °C, a second peak broad peak is observed at q ~0.06 – 0.07 Å^{-1}. The second peak is assigned as the second order as the position is around double that of the first order peak. The development of a second order peak suggest that the lamellar crystalline repeat structure is well developed and highly ordered in the draw PLLA samples [27, 53]. However, at T_d = 75 °C, no second order peak is observed in the 1D SAXS profiles and the first order peak at q ~ 0.03 Å^{-1} is broader that those at the other T_ds, which indicates that the crystalline lamellar structure is not as well developed in

this sample (as shown as well in the 2D SAXS/WAXS data (Figure 8) and orientation (Figure 9C)).

Correlation function analysis was performed on the 1D meridional SAXS profiles in Figure 10, to extract more detail about the crystalline lamellar morphology development in the PLLA samples during step annealing. Figure 11A shows example correlation functions for drawn PLLA samples at T_d = 60 °C and 65 °C and annealed at 90 °C. Figure 11B, shows the change in long period (L_p), which is the average repeat distance of crystalline and amorphous layers in the lamellar stacks, with annealing temperature of the drawn samples. As the annealing temperature increases, the L_p increases for all T_ds, which is verified in Figure 10, where the 1D SAXS peak position shifts to lower q with increasing annealing temperature [27, 54]. Figure 11C, shows the crystalline lamellar layer thickness, H_b, and as with L_p, this increases with annealing temperature, where the greatest lamellar thickness is seen where T_d = 60 – 65 °C at the annealing temperature of 160 °C. The increase in lamellar thickness is mirrored with increasing local crystallinity, as shown in Figure 11D. Here, the crystallinity increases most for T_d = 65 °C during the annealing process, but the final crystallinity for all T_ds at 160 °C tends to level-off at a value of ~40%.

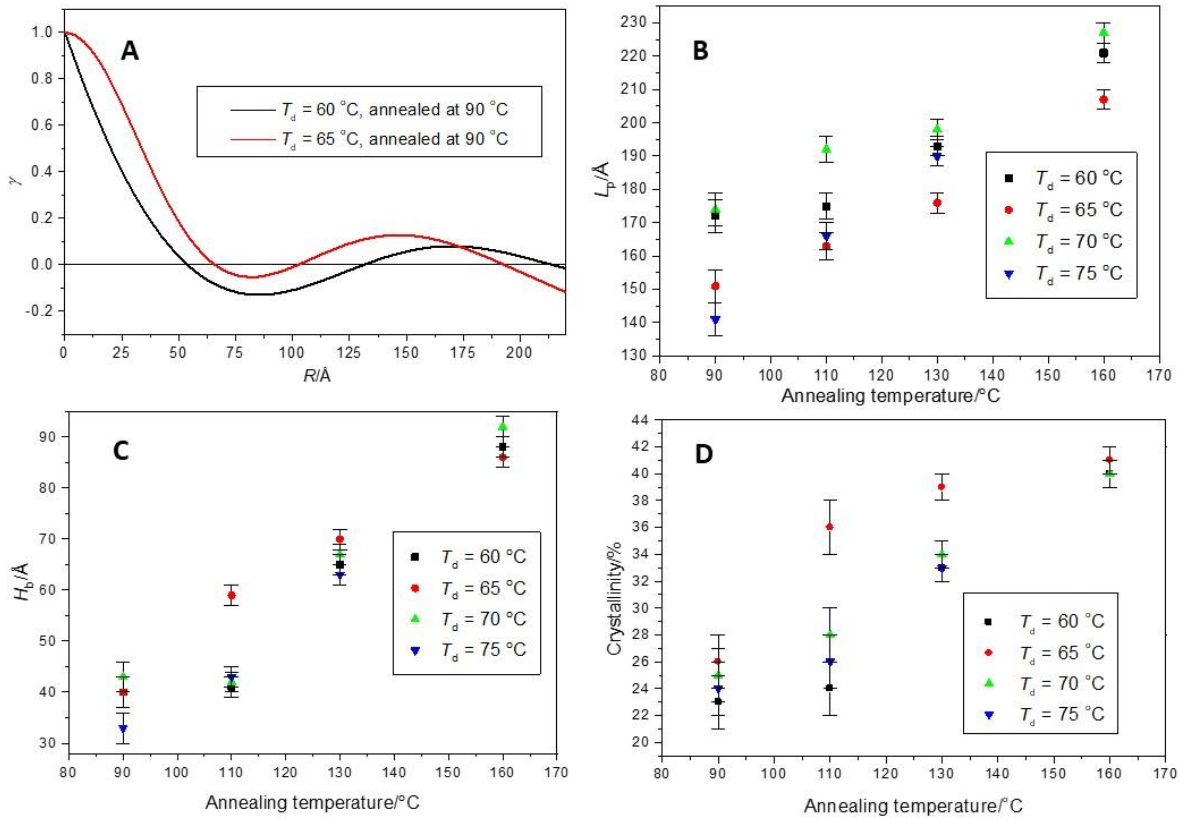

Figure 11: Correlation function analysis of PLLA 1D SAXS profiles. **A**: examples of computed correlation functions for PLLA post-draw at T_d = 60 °C annealed at 90 °C and T_d =

65 °C annealed at 90 °C; **B – D**: change in long period (L_p), change in crystalline layer thickness (H_b), change in local crystallinity with increasing annealing temperature, respectively.

Generally, the correlation function analysis of the 1D SAXS profiles has confirmed that the crystalline lamellar macrostructure develops in the PLLA samples as the annealing temperature increases, regardless of the T_d. The final crystallinity tends to a constant value for all samples at the maximum annealing temperature. However, to investigate the micromorphology development, in particular crystallite transitions that occur in the samples during annealing, a detailed analysis of the 1D WAXS is required.

3.5.3. Crystalline transitions from 1D WAXS

Figure 12A, shows 2D WAXS from the final frame of the draw (at 60 s) where the main diffraction peaks are indexed and their *hkl* values are labelled for the α/α' crystal forms.

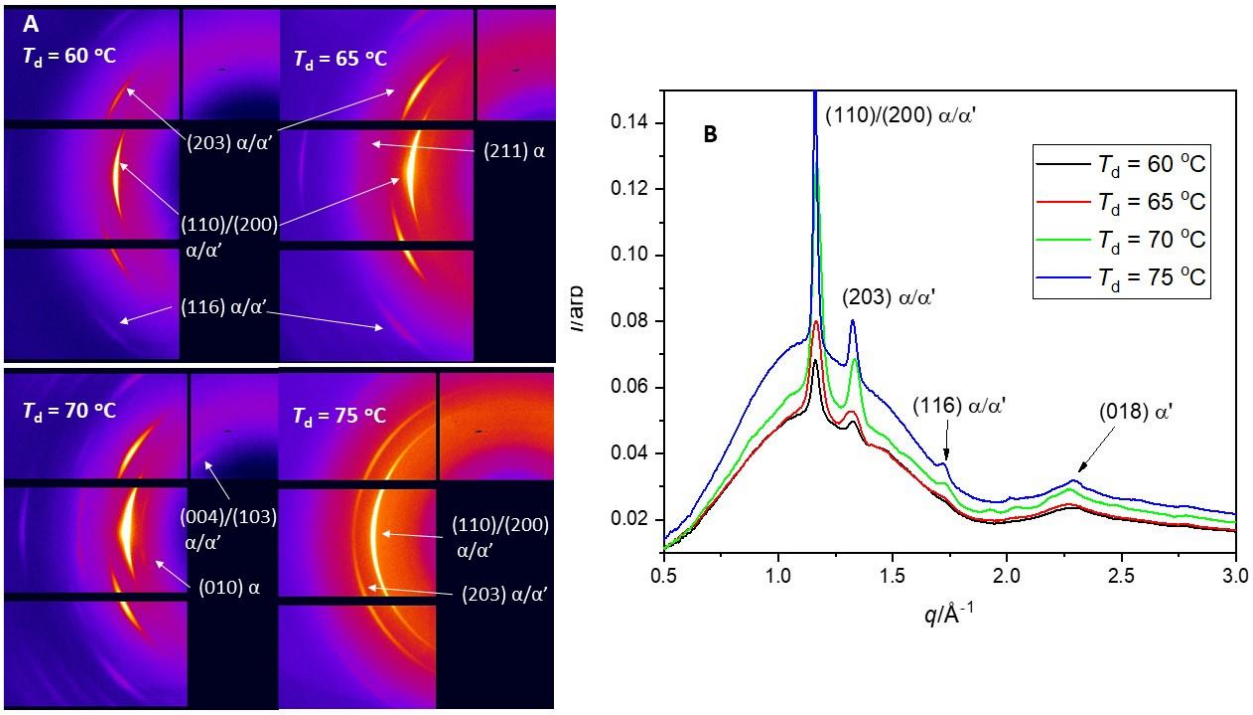

Figure 12. Final frame of the of the draw (60 s) at T_d between 60-65 °C **A:** 2D WAXS (the draw direction is vertical in all images); **B:** corresponding 1D WAXS profiles.

There are several differences in the final 2D WAXS from the draw; at T_d = 65 °C the main (110)/(200) and (203) diffraction arcs for the α/α' crystal forms are evident; as the T_d increases (65 – 70 °C) the patterns become more complex and more *hkl* diffraction arcs develop, which include more of those that relate to the stable α crystal form. The observation that the diffraction arcs for T_d between 60 - 70 °C are concentrated on the equator (horizontal

to the draw direction) indicates that the α/α' crystallites are well-oriented in the draw direction [21, 27]. In contrast, at T_d = 75 °C, the pattern shows mainly the (110)/(200) and (203) diffraction arcs for the α/α' crystal forms being slightly less complex that those at lower T_ds. Furthermore, the diffraction arcs have become more ring-like (increased azimuthal spread), indicating that the crystallites are not as well oriented (in the draw direction) in this sample. This is confirmed in the reduced lamellar stack orientation at this T_d as shown in Figure 9C. Figure 12B, shows the corresponding 1D profiles of the 2D WAXS patterns at all T_ds. Again, the main diffraction peaks for the α/α' crystal forms are labelled on the profiles. The 1D profiles also show a broad amorphous scattering peak centred at ~1.2 Å^{-1}, which appears to be more intense for the sample drawn at T_d = 75 °C (which is also obvious in the 2D WAXS), indicating that this sample is less crystalline than the others at lower T_ds post-draw. Hence, from the 1D WAXS profiles at the final frame of the draw, all samples show a mixture of the oriented α/α' crystal forms but the 1D SAXS (Fgure 10), indicates that no long-range lamellar morphology has developed at this stage.

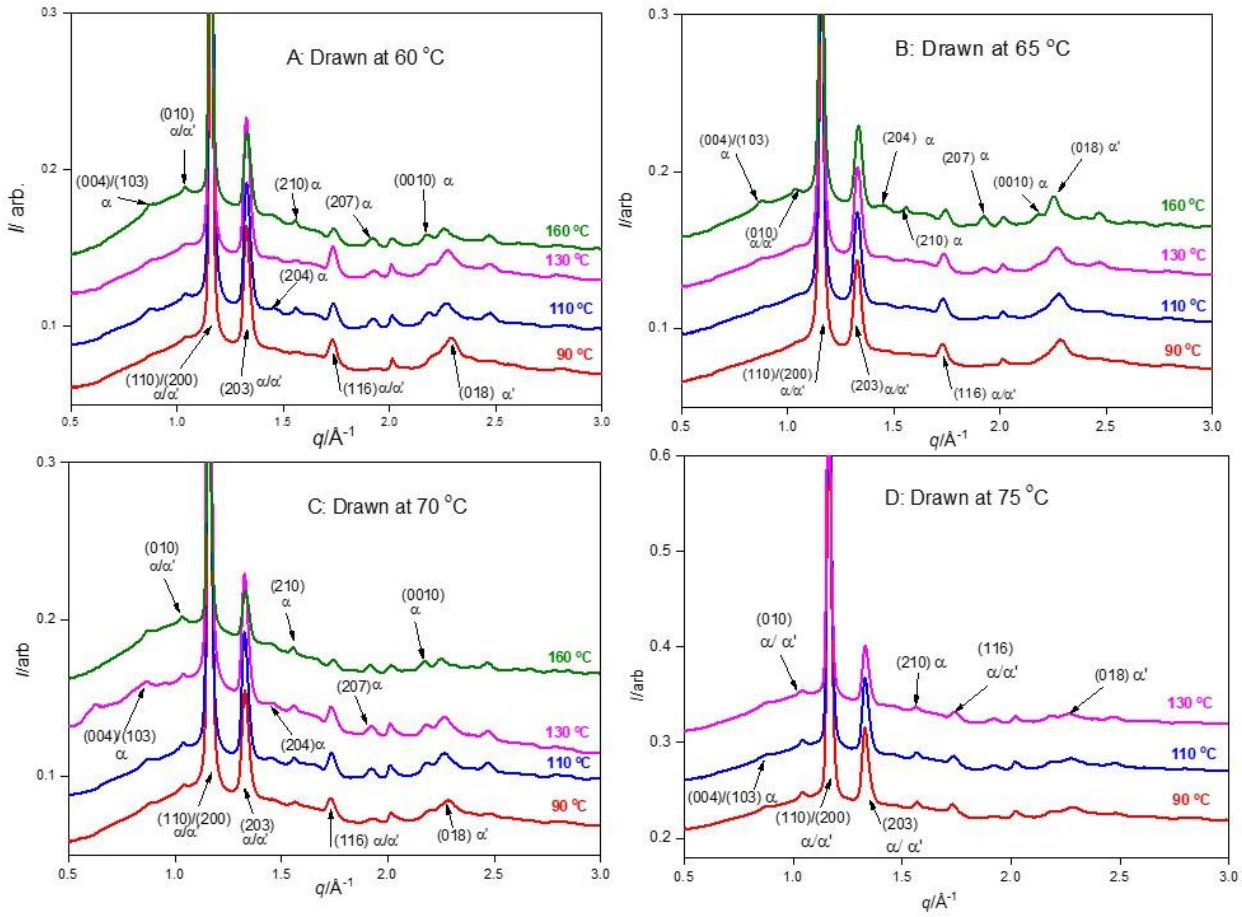

Figure 13. 1D WAXS profiles of PLLA drawn and step annealed up to 160 °C; **A**: T_d = 60 °C; **B**: T_d = 65 °C; **C**: T_d = 70 °C; **D**: T_d = 75 °C.

Therefore, to develop the crystal structure and enhance the amount of the α crystal form, the samples were annealed post-draw up to 160 ºC. Figure 13 shows the 1D WAXS profiles for all T_ds as the samples are step annealed with the peaks of the α/α' crystal forms labelled. At T_d = 60 ºC the 1D WAXS profile shows more peaks starting to emerge as the sample is annealed; at annealing temperatures between 110 - 130 ºC, several peaks which relate to the pure α crystalline form being indexed as (004)/(103), (204) and (210) start to develop, whereas the (116) and (018) α' peaks start to diminish in intensity. At 160 ºC, the (207) and (0010) peaks for the α crystalline form are now observed so there is a greater fraction of this crystal form present in the sample. Similarly, this is also observed for T_d 65 – 75 ºC (Figure 13B – 13D) where the 1D WAXS patterns become more complex with more peaks evolving as the annealing temperature increases, indicating the transformation of the least stable α' crystal to the more stable α crystalline form. Furthermore, the 1D SAXS analysis also confirms that the crystallinity and long-range lamellar ordering, also increases with increasing annealing temperature, during secondary processing.

4. Conclusions

Here we have combined mechanical testing with *in-situ* simultaneous SAXS/WAXS, thermal and SEM techniques to investigate the influence of T_d on the crystalline morphology and orientation development of PLLA during uniaxial drawing and how this structure then evolves during step annealing from secondary processing. The thermal and SAXS/WAXS data showed that the undrawn PLLA had some initial oriented crystalline structure which was generated from the injection moulding processing of the samples. From the mechanical testing at T_d = 60 ºC (being just below T_g), PLLA shows significant yielding and strain hardening behaviour, however T_ds between 60 – 75 ºC, idealised stress-strain behaviour is then observed. Thermal analysis of the post-drawn PLLA showed that the T_d does not alter the melting temperature, but the crystallinity increases at T_d > 65 ºC. During the drawing process, time resolved SAXS/WAXS showed that at low T_ds cavitation and voiding occurred and the initial crystallites underwent 'overdrawing' where they slip and are partially destroyed. SEM confirmed that surface voiding and cavitation had occurred at T_ds of 60 and 65 ºC but was absent at higher T_ds. However, no long-range macromolecular lamellar structure was seen post-draw, but small crystallites of the disordered α' crystal form of PLLA were observed. Therefore, to develop the crystalline lamellar structure and increase the amount of the stable α crystalline form, all the PLLA samples were step annealed in a second

processing stage. The SAXS/WAXS data showed that a highly oriented lamellar stack macrostructure developed on annealing, with increased crystallite size and crystallinity at all T_ds. Furthermore, step annealing drove the crystalline transition in all samples from the disordered α' crystal form to the stable α crystal form.

The results reported have confirmed that the injection moulding process produced some initial crystalline structure in the PLLA, which influenced the mechanical properties, crystallinity and crystalline phase transformation in PLLA during drawing and then throughout secondary processing. Therefore, varying pre- and post-processing parameters can significantly influence the orientation, crystal phase and micro- macromorphology of the final PLLA material.

Acknowledgements

ŁF would like to acknowledge the financial support from the EU through the Horizon 2020 Maria Skłodowska-Curie RISE project '*Biaxial stretching of PLLA-WS2 nanocomposites for thinner and stronger biomedical scaffolds*'. KB and NP gratefully acknowledge their PhD scholarships through the EPSRC Centre for Doctoral Training in Molecular Analytical Science (MAS), grant number EP/L015307/1. X-ray beam time at Diamond Light Source was provided under the experimental application SM16500-1. We are grateful for the assistance of all the Diamond I22 beamline staff.

References

[1] D. Garlotta, A Literature Review of Poly(Lactic Acid), Journal of Polymers and the Environment 9(2) (2001) 63-84.

[2] K. Hamad, Properties and Medical Applications of Polylactic Acid: A Review, eXPRESS Polymer Letters 9 (2015).

[3] M.S. Lopes, A.L. Jardini, R.M. Filho, Poly (Lactic Acid) Production for Tissue Engineering Applications, Procedia Engineering 42 (2012) 1402-1413.

[4] Y. Chen, L.M. Geever, J.A. Killion, J.G. Lyons, C.L. Higginbotham, D.M. Devine, Review of Multifarious Applications of Poly (Lactic Acid), Polymer-Plastics Technology and Engineering 55(10) (2016) 1057-1075.

[5] M. Fazita, K. Jayaraman, M.K. Haafiz, C. Saurabh, M.H. Hussin, A.K. H.P.S, Green Composites Made of Bamboo Fabric and Poly (Lactic) Acid for Packaging Applications—A Review, Materials 9 (2016) 435.

[6] A. Oz, Ö. Süfer, Y. celebi sezer, Poly (Lactic Acid) Films in Food Packaging Systems, Food Science & Nutrition Technology (FSNT) 2 (2017).

[7] E. Castro-Aguirre, F. Iñiguez-Franco, H. Samsudin, X. Fang, R. Auras, Poly(lactic acid)—Mass production, processing, industrial applications, and end of life, Advanced Drug Delivery Reviews 107 (2016) 333-366.
[8] S. Saeidlou, M.A. Huneault, H. Li, C.B. Park, Poly(lactic acid) crystallization, Progress in Polymer Science 37(12) (2012) 1657-1677.
[9] H. Tsuji, Poly(lactide) Stereocomplexes: Formation, Structure, Properties, Degradation, and Applications, Macromolecular bioscience 5 (2007) 569-97.
[10] H. Wang, J. Zhang, K. Tashiro, Phase Transition Mechanism of Poly(l-lactic acid) among the α, δ, and β Forms on the Basis of the Reinvestigated Crystal Structure of the β Form, Macromolecules 50(8) (2017) 3285-3300.
[11] P. De Santis, A.J. Kovacs, Molecular conformation of poly(S-lactic acid), Biopolymers 6(3) (1968) 299-306.
[12] B. Eling, S. Gogolewski, A.J. Pennings, Biodegradable materials of poly(l-lactic acid): 1. Melt-spun and solution-spun fibres, Polymer 23(11) (1982) 1587-1593.
[13] W. Hoogsteen, A.R. Postema, A.J. Pennings, G. Ten Brinke, P. Zugenmaier, Crystal structure, conformation and morphology of solution-spun poly(L-lactide) fibers, Macromolecules 23(2) (1990) 634-642.
[14] P. Pan, B. Zhu, W. Kai, T. Dong, Y. Inoue, Polymorphic Transition in Disordered Poly(l-lactide) Crystals Induced by Annealing at Elevated Temperatures, Macromolecules 41(12) (2008) 4296-4304.
[15] P. Pan, B. Zhu, W. Kai, T. Dong, Y. Inoue, Effect of crystallization temperature on crystal modifications and crystallization kinetics of poly(L-lactide), Journal of Applied Polymer Science 107(1) (2008) 54-62.
[16] L. Cartier, T. Okihara, Y. Ikada, H. Tsuji, J. Puiggali, B. Lotz, Epitaxial crystallization and crystalline polymorphism of polylactides, Polymer 41(25) (2000) 8909-8919.
[17] B. Lotz, G. Li, X. Chen, J. Puiggali, Crystal polymorphism of polylactides and poly (Pro-alt-CO): The metastable beta and gamma phases. Formation of homochiral PLLA phases in the PLLA/PDLA blends, Polymer 115 (2017) 204-210.
[18] X. Ou, M. Cakmak, Influence of biaxial stretching mode on the crystalline texture in polylactic acid films, Polymer 49(24) (2008) 5344-5352.
[19] G. Kokturk, E. Piskin, T. Serhatkulu, M. Cakmak, Evolution of phase behavior and orientation in uniaxially deformed polylactic acid films, Polymer Engineering & Science 42 (2002) 1619-1628.

[20] X. Ou, M. Cakmak, Comparative study on development of structural hierarchy in constrained annealed simultaneous and sequential biaxially stretched polylactic acid films, Polymer 51 (2010) 783-792.
[21] A. Mahendrasingam, D.J. Blundell, M. Parton, A.K. Wright, J. Rasburn, T. Narayanan, W. Fuller, Time resolved study of oriented crystallisation of poly(lactic acid) during rapid tensile deformation, Polymer 46(16) (2005) 6009-6015.
[22] G. Stoclet, R. Seguela, J.M. Lefebvre, S. Elkoun, C. Vanmansart, Strain-Induced Molecular Ordering in Polylactide upon Uniaxial Stretching, Macromolecules 43(3) (2010) 1488-1498.
[23] X. Zhang, K. Schneider, G. Liu, J. Chen, K. Brüning, D. Wang, M. Stamm, Structure variation of tensile-deformed amorphous poly(l-lactic acid): Effects of deformation rate and strain, Polymer 52(18) (2011) 4141-4149.
[24] X. Zhang, K. Schneider, G. Liu, J. Chen, K. Brüning, D. Wang, M. Stamm, Deformation-mediated superstructures and cavitation of poly (l-lactide): In-situ small-angle X-ray scattering study, Polymer 53(2) (2012) 648-656.
[25] Y. Wang, H. Zhang, M. Li, W. Cao, C. Liu, C. Shen, Orientation and structural development of semicrystalline poly(lactic acid) under uniaxial drawing assessed by infrared spectroscopy and X-ray diffraction, Polymer Testing 41 (2015) 163-171.
[26] A.C. Renouf-Glauser, J. Rose, D.F. Farrar, R.E. Cameron, The effect of crystallinity on the deformation mechanism and bulk mechanical properties of PLLA, Biomaterials 26(29) (2005) 5771-5782.
[27] K. Billimoria, E.L. Heeley, N. Parsons, Ł. Figiel, An investigation into the crystalline morphology transitions in poly-L-lactic acid (PLLA) under uniaxial deformation in the quasi-solid-state regime, European Polymer Journal 101 (2018) 127-139.
[28] Beamline-Soft Condenced Matter – Small Angle Scattering. , 2018. https://www.diamond.ac.uk/Instruments/Soft-Condensed-Matter/small-angle/I22.html. (Accessed 3/2/2020).
[29] D.J. Hughes, A. Mahendrasingam, C. Martin, W.B. Oatway, E.L. Heeley, S.J. Bingham, W. Fuller, An instrument for the collection of simultaneous small and wide angle x-ray scattering and stress–strain data during deformation of polymers at high strain rates using synchrotron radiation sources, Review of Scientific Instruments 70(10) (1999) 4051-4054.
[30] M. Basham, J. Filik, M.T. Wharmby, P.C.Y. Chang, B. El Kassaby, M. Gerring, J. Aishima, K. Levik, B.C.A. Pulford, I. Sikharulidze, D. Sneddon, M. Webber, S.S. Dhesi, F.

Maccherozzi, O. Svensson, S. Brockhauser, G. Naray, A.W. Ashton, Data Analysis WorkbeNch (DAWN), Journal of Synchrotron Radiation 22(3) (2015) 853-858.
[31] J. Filik, A.W. Ashton, P.C.Y. Chang, P.A. Chater, S.J. Day, M. Drakopoulos, M.W. Gerring, M.L. Hart, O.V. Magdysyuk, S. Michalik, A. Smith, C.C. Tang, N.J. Terrill, M.T. Wharmby, H. Wilhelm, Processing two-dimensional X-ray diffraction and small-angle scattering data in DAWN 2, Journal of Applied Crystallography 50(3) (2017) 959-966.
[32] FibreFix, 2018. https://www.diamond.ac.uk/Instruments/Soft-Condensed-Matter/small-angle/SAXS-Software/CCP13/FibreFix.html. (Accessed 3/2/2020).
[33] A.J. Ryan, SAXS Correlation Function: New Software at Daresbury Fibre Diffraction Review 3 (1994) 5.
[34] SasView for Small Angle Scattering Analysis, 2018. http://www.sasview.org/ (Accessed 3/2/2020).
[35] G. Porod, The small-angle X-ray scattering from densely packed colloidal systems, Kolloid-Zeitschrift 124(2) (1951) 31.
[36] F.J. Baltá-Calleja, C.G. Vonk, X-ray scattering of synthetic polymers, Elsevier1989.
[37] G.R. Strobl, M. Schneider, Direct evaluation of the electron density correlation function of partially crystalline polymers, Journal of Polymer Science: Polymer Physics Edition 18(6) (1980) 1343-1359.
[38] C.P. Buckley, C.Y. Lew, Biaxial hot-drawing of poly(ethylene terephthalate): An experimental study spanning the processing range, Polymer 52(8) (2011) 1803-1810.
[39] G. Kokturk, E. Piskin, T.F. Serhatkulu, M. Cakmak, Evolution of phase behavior and orientation in uniaxially deformed polylactic acid films, Polymer Engineering & Science 42(8) (2002) 1619-1628.
[40] J. Zhang, K. Tashiro, H. Tsuji, A.J. Domb, Disorder-to-Order Phase Transition and Multiple Melting Behavior of Poly(l-lactide) Investigated by Simultaneous Measurements of WAXD and DSC, Macromolecules 41(4) (2008) 1352-1357.
[41] T. Tábi, S. Hajba, J.G. Kovács, Effect of crystalline forms (α′ and α) of poly(lactic acid) on its mechanical, thermo-mechanical, heat deflection temperature and creep properties, European Polymer Journal 82 (2016) 232-243.
[42] C. Zhou, H. Guo, J. Li, S. Huang, H. Li, Y. Meng, D. Yu, J. de Claville Christiansen, S. Jiang, Temperature dependence of poly(lactic acid) mechanical properties, RSC Advances 6(114) (2016) 113762-113772.

[43] X. Shi, J. Qin, L. Wang, L. Ren, F. Rong, D. Li, R. Wang, G. Zhang, Introduction of stereocomplex crystallites of PLA for the solid and microcellular poly(lactide)/poly(butylene adipate-co-terephthalate) blends, RSC Advances 8(22) (2018) 11850-11861.
[44] F. Mai, W. Tu, E. Bilotti, T. Peijs, The Influence of Solid-State Drawing on Mechanical Properties and Hydrolytic Degradation of Melt-Spun Poly(Lactic Acid) (PLA) Tapes, Fibers 3(4) (2015) 523.
[45] E.W. Fischer, H.J. Sterzel, G. Wegner, Investigation of the structure of solution grown crystals of lactide copolymers by means of chemical reactions, Kolloid-Zeitschrift und Zeitschrift für Polymere 251(11) (1973) 980-990.
[46] D. Battegazzore, S. Bocchini, A. Frache, Crystallization kinetics of poly(lactic acid)-talc composites, Express Polym. Lett. 5 (2011) 849-858.
[47] A. Jalali, M. A. Huneault, S. Elkoun, Effect of thermal history on nucleation and crystallization of poly(lactic acid), 2016.
[48] A. Jalali, S. Shahbikian, M.A. Huneault, S. Elkoun, Effect of molecular weight on the shear-induced crystallization of poly(lactic acid), Polymer 112 (2017) 393-401.
[49] A. Pawlak, Plastic deformation and cavitation in semicrystalline polymers studied by X-ray methods, Polimery 59 (2014) 533-541.
[50] Y. Lu, Y. Men, Cavitation-Induced Stress Whitening in Semi-Crystalline Polymers, Macromolecular Materials and Engineering 303(11) (2018) 1800203.
[51] S. Röber, P. Bösecke, H.G. Zachmann, Small angle X-ray scattering pole figures of semicrystalline polymers obtained by synchrotron radiation, Makromolekulare Chemie. Macromolecular Symposia 15(1) (1988) 295-310.
[52] J.K. Lee, K.H. Lee, B.S. Jin, Structure development and biodegradability of uniaxially stretched poly(l-lactide), European Polymer Journal 37(5) (2001) 907-914.
[53] P. Xiao, H. Li, S. Huang, H. Wen, D. Yu, Y. Shang, J. Li, Z. Wu, L. An, S. Jiang, Shear effects on crystalline structures of poly(l-lactide), CrystEngComm 15(39) (2013) 7914-7925.
[54] T.-Y. Cho, G. Strobl, Temperature dependent variations in the lamellar structure of poly(l-lactide), Polymer 47(4) (2006) 1036-1043.